

Magnetic properties of defect-free and oxygen-deficient cubic SrCoO_{3-δ}Martin Hoffmann,^{1,2,*} Vladislav S. Borisov,^{1,2} Sergey Ostanin,² Ingrid Mertig,^{1,2} Wolfram Hergert,¹ and Arthur Ernst²¹*Institut für Physik, Martin-Luther-Universität Halle-Wittenberg, Von-Seckendorff-Platz 1, 06120 Halle, Germany*²*Max-Planck-Institut für Mikrostrukturphysik, Weinberg 2, 06120 Halle, Germany*

(Received 27 March 2015; revised manuscript received 31 July 2015; published 16 September 2015)

We investigated theoretically electronic and magnetic properties of the perovskite material SrCoO_{3-δ} with $\delta \leq 0.15$ using a projector-augmented plane-wave method and a Green's function method. This material is known from various experiments to be ferromagnetic with a Curie temperature of 260 K to 305 K and a magnetic moment of $1.5\mu_B$ to $3.0\mu_B$. Applying the magnetic force theorem as it is formulated within the Green's function method, we calculated for SrCoO_{3-δ} the magnetic exchange interactions and estimated the Curie temperature. Including correlation effects by an effective U parameter within the GGA + U approach and verifying this by hybrid functional calculations, we obtained the Curie temperatures in dependence of the oxygen deficiency close to the experimental values.

DOI: [10.1103/PhysRevB.92.094427](https://doi.org/10.1103/PhysRevB.92.094427)

PACS number(s): 61.72.jd, 71.15.Mb, 71.70.Gm, 75.47.Lx

I. INTRODUCTION

Perovskite materials with the simple structure formula ABO_3 attracted attention in the past decades because of potential applications in spintronics. Especially ferromagnetic metallic perovskites have rekindled interest, since they can be used as electrodes in complex oxide heterostructures, while conventional ferromagnetic materials such as $3d$ transition metals are hardly compatible with most of the oxides.

Over the past years, advanced experimental growing techniques allow for the growth of heterostructures and multilayer systems with a huge variety of properties, e.g., multiferroic, magnetoelectric, or magneto-optic. Out of this class of materials, we concentrated on SrCoO_{3-δ} (SCO) with a possible oxygen deficiency δ . In its pure single-crystal composition, the experiments verify ferromagnetic behavior up to room temperature and metallic conductance [1]. Metallic oxides are highly desired for contacts and electrodes of the above discussed multifunctional heterostructures because of a good lattice match between the electrode and the top layer oxide. Undesired distortions of thin layers could be reduced. Simultaneously, it is possible to transport an electric current, e.g., in the compounds SrCo_{1-x}Fe_xO₃ for $x \leq 0.5$, which are particularly suitable as electrode materials for solid electrolyte oxygen sensors [2]. In addition, complex oxides based on SrCoO₃ like, e.g., La_{0.6}Sr_{0.4}CoO₃ or SrCo_{0.9}Sb_{0.1}O_{3-δ} appear to be particularly useful as cathodes for intermediate-to-low temperature solid oxide fuel cells [3,4].

In the literature there are several experimental investigations and theoretical studies on SCO. They all verify the ferromagnetic and metallic behavior of this material. In theory, in particular, the electronic structure [5–7], the spin state [8,9], and possible lattice distortions [10] are thoroughly discussed. Potze *et al.* [8] show that SrCoO₃ exhibits an intermediate spin (IS) state due to the competition of intra-atomic exchange and the cubic crystal field. Such an IS-state may be understood as a high spin state of a Co³⁺ ion antiferromagnetically coupled to a ligand hole of e_g symmetry (notation from Ref. [8]: $d^6\bar{L}_{e_g}$). A more recent study identified this high spin state as d^6 , but

it is mixed with several other possible spin states [9]. Also the magnetic moment (ranging from $2.6\mu_B$ to $3.19\mu_B$) [7,10] is reproduced by theory and close to $3\mu_B$, which agrees very well with the IS-state picture ($S = 3/2$).

However, there is only one paper which discussed the Curie temperature (T_C) of SrCoO₃ from a theoretical point of view ($T_C \approx 1800$ K) [9]. This value is far too high in comparison to the experimentally measured values, which vary from 212 K to 305 K [1,11–15]. This variation might result from different synthesis techniques and defects. Usually, the cubic and stoichiometric phase SrCoO₃ is prepared from the brownmillerite phase SrCoO_{2.5} [1]. The oxidation is either done by a high oxygen pressure during the heating [1] or by electrochemical oxidation [13,16]. Furthermore, most samples are polycrystalline and the oxygen amount is smaller than the nominal value ($\delta \geq 0.05$). The cubic structure is only stable for a narrow range of δ , since SCO forms a homologous series (SrCoO_{(3n-1)/n}) for δ from 0.5 to 0 and changes its structure from orthorhombic via cubic and tetragonal to cubic again [17–19]. Even for this cubic range close to $\delta = 0$, the lattice constant increases slightly with decreasing oxygen content [15,16,18,20,21], whereas the critical temperature decreases from 292 K to 182 K [15,21]. Anyway, these values for polycrystalline samples are smaller than for a single crystal ($T_C = 305$ K and $\delta = 0.05$) [1]. As for the T_C values, the measurements of the magnetic moments vary for different experiments between $1.2\mu_B$ and $2.6\mu_B$ [1,11,13].

Therefore, we studied in this work the electronic and magnetic properties of SCO from *ab initio*. There were strong indications for the IS-state proposed by Potze *et al.* [8], when using in the calculations more advanced exchange-correlation functionals other than the generalized-gradient approximation. Thereby, the theoretically estimated critical temperature as well as its reduction with increasing amount of oxygen vacancies (V_O) agreed well with the experimental observations.

In the following, we start with a detailed description of the studied structure and the applied theoretical methods. The results are discussed at first for the defect-free SCO. Afterwards, we extend our study also to oxygen vacancies in SCO. We close this work with a summary.

*mart.hoffi@gmail.com

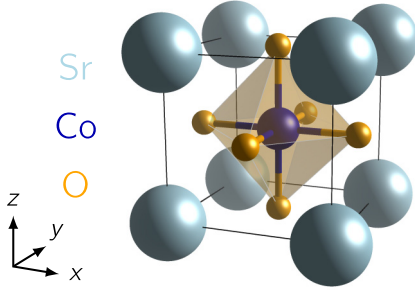


FIG. 1. (Color online) Structure of the cubic phase of SrCoO₃. Picture was created with VESTA [22].

II. COMPUTATIONAL DETAILS

In this work, the calculations were performed for a primitive cubic cell of SrCoO₃ (see Fig. 1). To study structural, electronic, and magnetic properties of SrCoO₃, we performed extensive first-principles calculations within density functional theory and combined two methods, which have been proven to be very reliable in this particular context. The projector-augmented plane-wave method of the Vienna *ab initio* simulation package (VASP) [23–25] was used for the calculation of total energies and structural relaxation to search for possible deviations from the cubic structure. The main results were obtained with the Korringa-Kohn-Rostoker Green’s function (GF) method HUTSEPOT. HUTSEPOT is developed by Ernst *et al.* at the Max Planck Institute of Microstructure Physics, Germany. Its basic features were described in [26]. In both methods, if not particularly stated otherwise, the generalized-gradient approximation (GGA) [27] was used and we considered the electronic correlation effects for the *d* orbitals of Co with an additional Hubbard *U* within the GGA + *U* approach [28] in the implementation of Dudarev *et al.* [29]. The $U_{\text{eff}} = U - J$ was applied as a parameter varying from 0 eV to 9 eV.

A. Structural relaxation

The plane-wave basis for the VASP calculations was taken with a cutoff energy of 460 eV and a Γ -centered ($8 \times 8 \times 8$) *k* mesh was used. It reproduced the experimental unit cell volume of Ref. [13] (cubic phase; $a_{\text{ref}} = 3.835 \text{ \AA}$) with a deviation of less than 3% for the studied range of U_{eff} . In the same order of magnitude or smaller are the differences (with respect to a_{ref}) to the single-crystal lattice constant [1] $a_{\text{sngl}} = 3.8289 \text{ \AA}$ [$\Delta V = -0.47\%$ with $V = (a_{\text{sngl}})^3$] or possible variations due to oxygen vacancies observed, e.g., in Ref. [15] ($\Delta V = +2.2\%$) or Ref. [16] ($\Delta V = +0.56\%$) (see overview in Fig. 2). For the sake of completeness, we compared our GGA results with hybrid functional calculations using the common HSE03 functional [30], available within VASP but at the moment not available in the GF method. In the HSE03 functional, the mixing $\alpha = 0.25$ and the screening parameter $\mu = 0.3 \text{ \AA}^{-1}$ are chosen for the Hartree-Fock exchange energy. Because of the high computational demands of such type of calculations, the cutoff energy was reduced to 400 eV and the Γ -centered *k* mesh was only $4 \times 4 \times 4$. The lattice relaxation provided for a cubic phase the equilibrium lattice

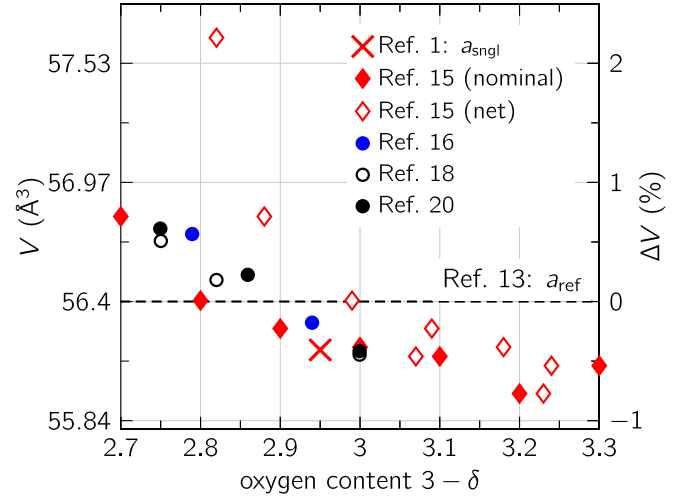


FIG. 2. (Color online) Experimental lattice volume as a function of oxygen concentration from several references. The change of the volume is $\Delta V = (V - a_{\text{ref}}^3)/a_{\text{ref}}^3$ with respect to $a_{\text{ref}} = 3.835 \text{ \AA}$ (black dashed line). The nominal and net values of Ref. [15] represent the provided and measured oxygen content.

parameter $a_{\text{HSE03}} = 3.833 \text{ \AA}$, which is in very good agreement with the experimental values shown above. Although we did not observe any indication of a tetragonal distortion in our GGA + *U* calculations, we found by applying the HSE03 exchange functional that the *a/c* ratio deviated by few percent from 1. Since the experiments for stoichiometric SrCoO₃ did not observe a tetragonal unit cell and the electronic structure did not change substantially with respect to the cubic phase, we stayed in the main part of the paper consistently with the cubic SCO and the lattice constant $a_{\text{ref}} = 3.835 \text{ \AA}$ and investigated a hydrostatic volume variation separately in Sec. III D.

B. Magnetic properties with the Green’s function and Monte Carlo method

The calculations with the GF method were performed within the full charge density approximation, which takes into account the nonsphericity of the charge density and improved the accuracy of calculations for complex unit cell geometries.

The GF method, which is based on the multiple scattering theory, allows the calculation of the magnetic exchange interactions J_{ij} between the magnetic atoms at site *i* or *j* by using the magnetic force theorem [31]. Therein, the magnetic moments at *i* and *j* of an ordered magnetic structure are rotated against each other about a small angle. From the resulting energy variation follows

$$J_{ij} = \frac{1}{8\pi} \int_{\epsilon}^{E_F} d\epsilon \text{Im Tr}_L (\Delta_i \hat{\tau}_\uparrow^{ij} \Delta_j \hat{\tau}_\downarrow^{ji} + \Delta_i \hat{\tau}_\downarrow^{ij} \Delta_j \hat{\tau}_\uparrow^{ji}), \quad (1)$$

where $\hat{\tau}^{ij}$ is the scattering path operator and $\Delta_i = \hat{\tau}_{i\uparrow}^{-1} - \hat{\tau}_{i\downarrow}^{-1}$ the difference between the spin-dependent single scattering operators of site *i*. The trace is taken over all relevant angular momentum quantum numbers $L = (l, m)$.

The J_{ij} from (1) enter a classical Heisenberg Hamiltonian,

$$\hat{H} = - \sum_{i,j} J_{ij} \mathbf{S}_i \cdot \mathbf{S}_j, \quad (2)$$

with the magnetic moments S_i and S_j . The model Hamiltonian (2) allows an estimate of the critical temperature \tilde{T} with a Monte Carlo (MC) simulation. Here, \tilde{T}^{MC} might mark the transition to any kind of magnetic ground state, which might result from the calculations. We cross checked our results with the mean-field approximation (MFA) and the well-established random phase approximation (RPA) [32]. All three methods showed a similar tendency in the variation of \tilde{T} with respect to the considered influences like electron correlations or oxygen vacancies. Since the MFA is known to overestimate \tilde{T} , we restricted the discussion to the MC results. For the particular MC simulations, we choose 8000 magnetic atoms in a cluster with periodic boundary conditions. The temperature was reduced in steps of 5 K starting from a high-temperature disordered state above \tilde{T}^{MC} . At every temperature T , we assumed that the thermal equilibrium was reached after 20 000 MC steps and after 20 000 additional MC steps thermal averages were calculated. \tilde{T}^{MC} was then obtained from the fitting of the temperature dependency of the magnetic susceptibility, cross checked by the temperature dependence of the saturation magnetization and the heat capacity. The obtained transition temperatures were determined within a numerical uncertainty range of ± 5 K. Further computational details of our MC scheme can be found in Refs. [33–35]. From the orientation of the magnetic moments at low temperatures and the spin-spin correlation function, we deduced the magnetic ground state of the simulated system, which was not only ferromagnetic (FM) with the Curie temperature, T_C , as observed from the experiments, but also antiferromagnetic (AFM) with the Néel temperature, T_N , or a more complicated noncollinear ferrimagnetic (FiM) spin arrangement with a transition temperature, \tilde{T} , and potentially with a saturation magnetization of zero. We introduced those labels for the different magnetic transitions for the sake of clarity throughout our work and speak of \tilde{T} if the ground state is not clarified.

In our calculations for a FM ground state (reference state, RS_{FM}), we found besides the magnetic cobalt ions small induced moments at the oxygen sites. Since those moments disappear usually at and above the magnetic transition temperature, their magnetic coupling can lead to a wrong estimation of the critical temperature. We compared the results of (1) for the FM reference state RS_{FM} with the magnetic coupling constants obtained at a high-temperature paramagnetic (PM) reference state (RS_{PM}). Such state can be modeled successfully with the disordered local moment (DLM) theory using the GF method [36,37]. Here arrangements of local magnetic moments $\{S_i\}$ at the sites i are thought to fluctuate independently. Above \tilde{T} , the orientations of those local moments are randomly distributed and the average magnetization per site is zero. Hence, the induced moments vanish. From the computational point of view, the coherent potential approximation (CPA) [38], as it is implemented within the multiple scattering theory [39], can be used to model the susceptibility or the electronic structure for such disordered magnetic systems [36,37]. With respect to the calculation of the J_{ij} in (1), the scattering path operators $\hat{\tau}^{ij}$ of the perfect magnetic ordering will be exchanged with the ones of the effective CPA medium $\hat{\tau}_C^{ij}$. The random orientation of the magnetic moments in the DLM picture causes usually an increase in the size of the orbitals. Therefore, the magnetic coupling is usually stronger in the case of a DLM calculation

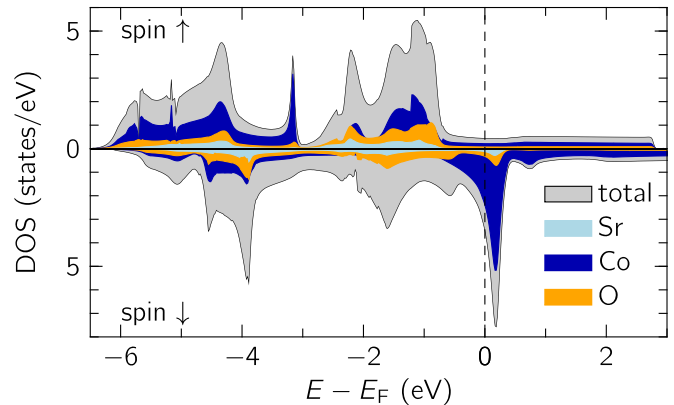


FIG. 3. (Color online) Atomic and spin-resolved density of states of SrCoO_3 with contributions of each species and spin-up (top panel) and spin-down (bottom panel) obtained with the GF method (GGA). The oxygen p states at all three oxygen ions in the unit cell are threefold degenerate (only one is shown). The main features of the LDOS are similar in VASP (not shown).

since the strength of the magnetic coupling is proportional to the overlap between the contributing orbitals. This means for the resulting transition temperature that it can become either larger or smaller depending on the type of magnetic exchange, e.g., a reduction for AFM (super-) exchange.

To describe the oxygen-deficient SCO in the GF method, we applied also the CPA using a certain amount (δ) of empty spheres at the oxygen sites to mimic V_O . However, vacancies may lead to substantial relaxations of the underlying crystal structure. We did not account for such structural deformations in our CPA calculations but investigated their impact on the magnetic interaction using a supercell approach with the GF method. We found only minor changes in the exchange constant values and, therefore, the discussion below reports results from the ideal cubic structure.

III. RESULTS

A. Defect-free SCO

We investigated at first the electronic properties of SrCoO_3 for the experimental lattice constant. Due to the oxygen octahedron, which surrounds the Co ion, the d states of cobalt experience a crystal-field splitting of cubic symmetry, which results in three t_{2g} and two e_g degenerated states. The orbitals corresponding to the e_g states are oriented along the coordinate axes pointing to the oxygen ions and those corresponding to the t_{2g} states are pointing to the next nearest-neighboring Co ions (see Fig. 1).

The local density of states (LDOS) within the GGA shows for VASP and HUTSEPOT an almost fully occupied majority spin channel and a pronounced peak of the Co t_{2g} spin-down states at the Fermi energy E_F (see Fig. 3). All other cobalt $3d$ states— e_g^\uparrow , t_{2g}^\uparrow , and e_g^\downarrow —are below the E_F and smeared over a large energy range due to a strong hybridization with the p states of oxygen. This is in a good agreement with previous results [9] but contradicts the IS-state picture with particular occupied and unoccupied t_{2g} Co states ($t_{2g}^4 e_g^1$) [8].

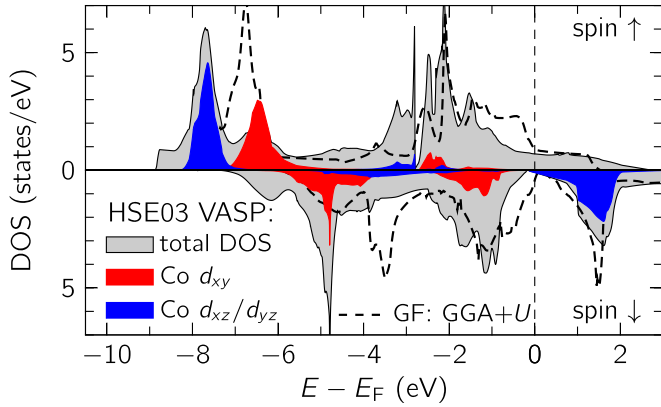


FIG. 4. (Color online) Spin-resolved density of states of SrCoO_3 in the spin-up (top panel) and spin-down channels (bottom panel) obtained with VASP (HSE03 functional) and GF method (GGA + U with $U_{\text{eff}} = 5$ eV). Only the nondegenerated Co 3d states are shown.

The total moment of this IS-state model would be theoretically $3\mu_B$ ($s = 3/2$). Although the total magnetic moment of $\mu = 2.281\mu_B$ calculated with the GF method and the GGA functional was smaller than in the IS-state model, it agreed well with the range of the experimentally observed magnetic moments ($\mu \approx 2\mu_B$ to $2.5\mu_B$). The main contribution to the total moment originated correctly from the Co ions with only small induced moments of $0.15\mu_B$ and $0.04\mu_B$ at the oxygen and strontium ions, respectively. The discrepancy between the IS-state model and the experiments was always attributed to possible defects. However, when the IS-state model is valid, theoretical calculations of a defect-free SCO should reproduce the total magnetic moment.

Possible shortcomings might originate from the GGA electron correlation functional, which often lacks a sufficient description of localized transition metal d states. For comparison, we calculated the total magnetic moment and the DOS of SCO also with the hybrid functional HSE03 available in VASP. The obtained total magnetic moment of $2.9\mu_B$ within VASP and the HSE03 functional agreed well with the IS-state model. Additionally, the DOS showed also the expected orbital occupation $t_{2g}^4 e_g^1$ of the Co states: two unoccupied t_{2g}^\downarrow (d_{xz} and d_{yz} above E_F) and one occupied t_{2g}^\downarrow state (d_{xy} below E_F) (see Fig. 4).

We have to note that due to the symmetric cubic structure, the particular localization of d_{xy}^\downarrow is arbitrary and depends on the starting point of the self-consistent calculation. Another localized Co d^\downarrow state is also possible and was observed during the calculations. However, for a consistent description we continued throughout this work with one particular configuration (the singlet d_{xy}^\downarrow state).

In order to calculate the critical temperature, the magnetic exchange interactions for the nearest-neighbor atoms were calculated with the GF method and the GGA functional. For RS_{FM} the magnetic interaction parameters show mainly a FM (positive) coupling: strong between two adjacent Co ions and much weaker between the Co ions and the induced magnetic moments of the surrounding oxygen ions (see Fig. 5). The coupling to the Sr ions was one order of magnitude

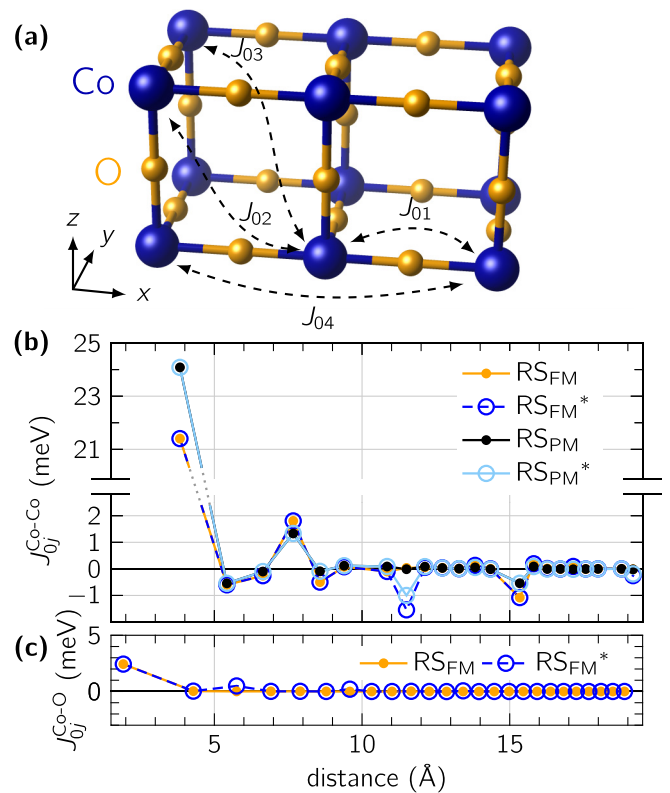


FIG. 5. (Color online) (a) Schematic view of the orientation of the first magnetic exchange interactions J_{ij} only between the Co ions. The nonmagnetic Sr ions are not shown. The notation J_{01} , J_{02} , ... means nearest neighbors, next-nearest neighbors, etc. Below, the values for the coupling between Co-Co and Co-O are given in (b) and (c), respectively. Both are calculated with the GF method (GGA) for a FM and PM (DLM model) reference state, respectively. The asterisk marks those coupling constants which strictly follow only one direction in space [along a single cube edge in (a)]. The abscissa in (b) is noncontinuous, due to the large differences in the values.

smaller and was ignored in the following discussions. After the eighth shell ($d = 7.7$ Å), most of the coupling constants decay fast while other long-range interactions reflect the metallic character of SrCoO_3 . Along the straight exchange paths (along a particular coordination axis, also marked with an asterisk in Fig. 5) the coupling via the oxygen ions remains stronger. The same tendency can be observed for the coupling between the Co ions in the DLM model (J_{ij} calculated with RS_{PM}). Only the nearest-neighbor interactions became larger while the other coupling constants were reduced. At the oxygen ions, the induced magnetic moments vanished in the DLM model and no exchange interactions were found between them. In the MC method, we took into account all coupling constants up to the distance of 15.34 Å. The resulting Curie temperature did not agree with the experimental results (within the DLM model $T_C^{\text{MC}} = 771$ K compared to $T_C^{\text{exp}} \approx 280$ K). The reason for this high T_C^{MC} might be an overestimation of the magnetic coupling between the Co atoms. The increase in the localization of 3d states by using electron correlation corrections or more advanced functionals should decrease as well the orbital overlap and thereby reduce the exchange coupling.

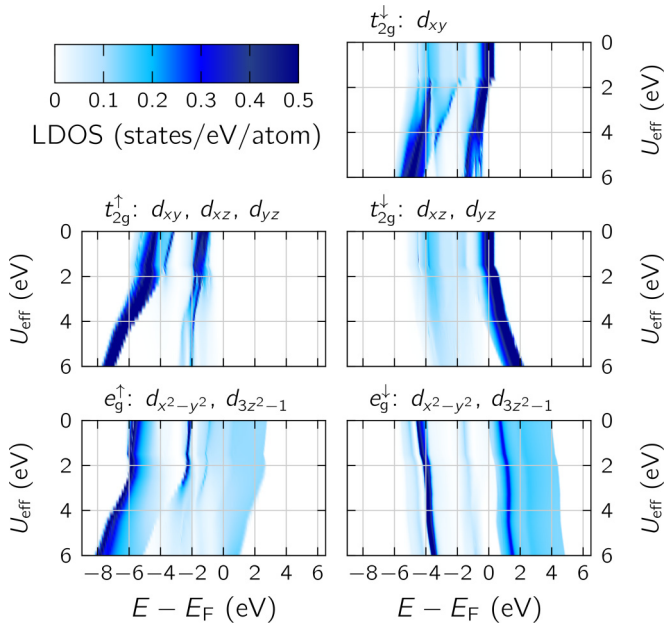


FIG. 6. (Color online) Contour plots of the LDOS in the ground state for the Co d states in dependence of the correlation parameter U_{eff} (ordinate) obtained with the GF method. They are spin resolved (left, up; right, down) and collected according to their initial degeneracy. For higher U_{eff} (not shown), the energy shift continues and there are no significant changes to observe.

In summary, the DOS, the total magnetic moment, and the critical temperature illustrate the need for electron correlation corrections for the description of the properties of SCO. Unfortunately, the calculations with hybrid functionals consume large amounts of computational resources and were also at the moment not available within HUTSEPOT, which was needed for the calculations of the J_{ij} . However, the parametric GGA + U approach was less time consuming and provided similar results, as discussed in Sec. III B. For that reason, we stayed for the remainder of this work with the GGA + U method. Additionally, we describe also the oxygen-deficient material, where we expect a reduction of the critical temperature and a slightly enhanced volume [15].

B. Electronic correlation corrections

The common way to consider the electronic correlations within the GGA + U method is to optimize the value of the repulsive U_{eff} with respect to the experimental data for structural and magnetic properties of the system. As we see from former studies, the value of U_{eff} might range from 2.5 eV (Ref. [10]) to 8 eV (Ref. [7]). The constrained RPA provided a value of $U = 10.83$ eV and $J = 0.76$ eV for the Co d states [9], which seems to be too high for a metallic system.

Since the correct value of U_{eff} is hard to estimate from first-principles and the above reference values scatter quite a bit, we investigated the electronic structure and the occupation of the Co d states for the whole range of U_{eff} from 0 eV to 9 eV with the GF method (see Fig. 6). Interestingly, for the first few steps of the calculations ($U_{\text{eff}} \leq 1.5$ eV) the d states preserve their degeneracy in t_{2g} and e_g states. At the Fermi energy E_F , the large peak of the Co t_{2g} states does not move due to

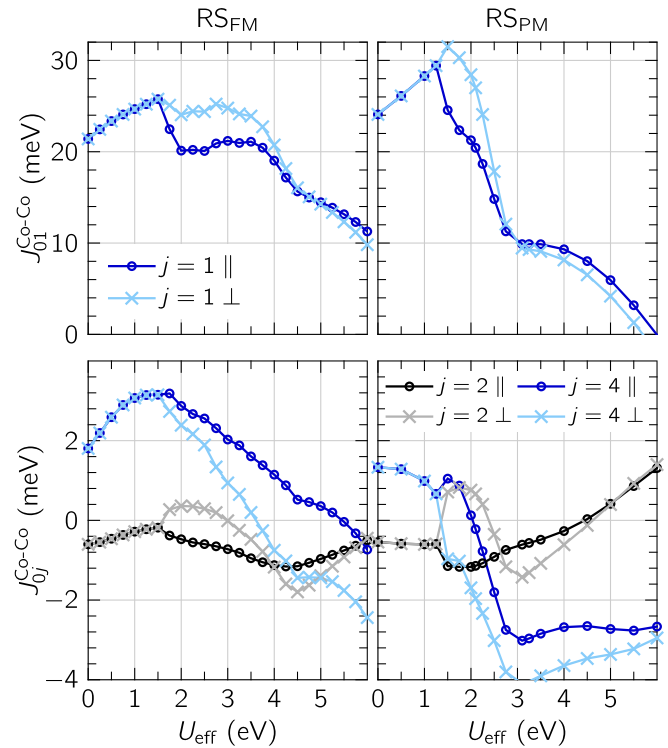


FIG. 7. (Color online) The magnetic exchange interactions $J_{0j}^{\text{Co-Co}}$ as a function of U_{eff} for a FM (left) or PM (right) reference system. They are subdivided into two groups, \parallel and \perp , for $J_{0j}^{\text{Co-Co}}$ only in the x - y plane and those with contributions also in x direction [directions given in Fig. 5(a)]. The $J_{03}^{\text{Co-Co}}$ (not shown) does not split due to U_{eff} and are always small (< 0.3 meV).

an interplay of the Coulomb exchange and the crystal-field energy. Only for a larger U_{eff} , the degeneracy is lifted as it was observed before in the DOS calculated with the HSE03 (see Fig. 4). A singlet state (d_{xy}^{\downarrow}) becomes occupied while the doublet (d_{xz}^{\downarrow} and d_{yz}^{\downarrow}) is pushed above E_F . On the other hand, in the spin-up channel the orbitals remain degenerate for the whole range of U_{eff} and become strongly localized (see much higher contrast for d_{xy}^{\uparrow} in Fig. 6). It matches well with $t_{2g}^4 e_g^1$ and the IS-state model.

A similar loss of degeneracy in the $3d$ states was also observed in calculations with VASP and GGA + U , but at higher values for U_{eff} than in the GF method (happening between 5 to 7 eV, not shown). Furthermore, we obtained a very good agreement of the electronic structure around the E_F , calculated either with the GF method at $U_{\text{eff}} = 5$ eV or with VASP (HSE03) (see Fig. 4). For states further below E_F , the differences become larger but those states contribute only little to the orbital overlap needed for the calculation of magnetic exchange parameters with the magnetic force theorem.

For the understanding of the critical temperature, we calculated with the GF method the magnetic coupling parameters J_{ij} for the FM and PM (DLM model) reference state, respectively (see Fig. 7). Both reflect the change in the degeneracy of the Co d state in the LDOS. Due to the splitting of the t_{2g}^{\downarrow} states into the degenerated doublet (d_{xz}^{\downarrow} and d_{yz}^{\downarrow}) and a singlet (d_{xy}^{\downarrow}), the J_{ij} with either (\parallel) in x and y direction or (\perp) in z direction were

different for $U_{\text{eff}} > 1.5$ eV. For the ground-state calculation (RS_{FM}), the most dominant coupling constants, $J_{01}^{\text{Co-Co}}$ and $J_{04}^{\text{Co-Co}}$, are strongly FM (see left-hand side in Fig. 7). Both interactions are mediated by oxygen ions between Co ions forming either a Co-O-Co or a Co-O-Co-O-Co chain (see inset in Fig. 5). Those bonds connect mostly the O p states with the Co e_g states (σ bonds). This typically AFM superexchange is suppressed by the metallic character of SrCoO₃ and we observe band magnetism. In the degenerated parameter region, the coupling becomes even stronger with U_{eff} until 1.5 eV because the Co e_g^\uparrow and e_g^\downarrow states are either pushed below or above E_F , respectively. This increases the exchange splitting and, therefore, the magnetic coupling. In contrast, the coupling between two Co ions enclosing a 90° angle ($J_{02}^{\text{Co-Co}}$) is small and AFM, while the next coupling ($J_{03}^{\text{Co-Co}}$) is very weak compared to the other interactions.

After that, in the symmetry-broken regime, the competing superexchange overcomes the band magnetism and we observed an increasing localization of the d states (see stronger contrast in Fig. 6). This reduces, in general, the overlap of the orbitals and the magnetic exchange interactions. It is visible, e.g., for J_{01} and J_{04} in Fig. 7 but also for other J_{0j} (not shown). On the other hand, the modifications in the coupling constants are much more complex due to the changing LDOS. However, some simple tendencies can be observed, e.g., due to the localization of the Co d_{xy} states, the magnetic coupling for $U_{\text{eff}} < 4$ eV in the x - y plane (\parallel contributions in J_{01}) becomes smaller than the out-of-plane (\perp) contributions. The \perp parts of $J_{02}^{\text{Co-Co}}$ even change their character from AFM to FM. Another significant change for all coupling constants is visible at $U_{\text{eff}} = 4.5$ eV and might be correlated with vanished states in the d_{xy} LDOS indicated by a loss of contrast (see Fig. 6). At the end of the shown range, the strength of the nearest-neighbor magnetic exchange coupling was only half of its starting value. It reduces further for even higher U_{eff} (not shown) and leads to an undesired AFM ground state.

The overall tendencies for the RS_{FM} calculations were in general also observed in the DLM picture (RS_{PM}), although the changes were much stronger; e.g., at $U_{\text{eff}} = 6$ eV the J_{01} were reduced to zero and J_{04} is strongly AFM. Furthermore, the loss of degeneracy was visible already for smaller U_{eff} (see Fig. 7). Both changes are explained by the larger extent of the Co d orbital due to the random distribution of the magnetic moments in the DLM theory, as already stated in Sec. II. The increasing orbital overlap enhances, on the one hand, the AFM superexchange and, on the other hand, alters the competition between the crystal field and Coulomb energy which restored the degeneracy for small U_{eff} .

The critical temperatures obtained from the MC simulation using the magnetic exchange parameters in the RS_{FM} or with the DLM model follow, in general, a similar tendency as the nearest-neighbor coupling constant $J_{01}^{\text{Co-Co}}$ (see Fig. 8). They show for both sets of magnetic coupling parameters a linear increase up to $U_{\text{eff}} = 1.5$ eV. The critical temperatures obtained with the J_{0j} (RS_{FM}) remained around 750 K with increasing U_{eff} up to ≈ 3 eV and drop down sharply in the following while the DLM results decrease linearly immediately above 1.5 eV. So, $\tilde{T}^{\text{MC}}(U_{\text{eff}})$ calculated for RS_{PM} reaches the experimentally relevant range already for a smaller $U_{\text{eff}} = 2.5$ eV than for RS_{FM} (4.5 eV). A reason for the smaller

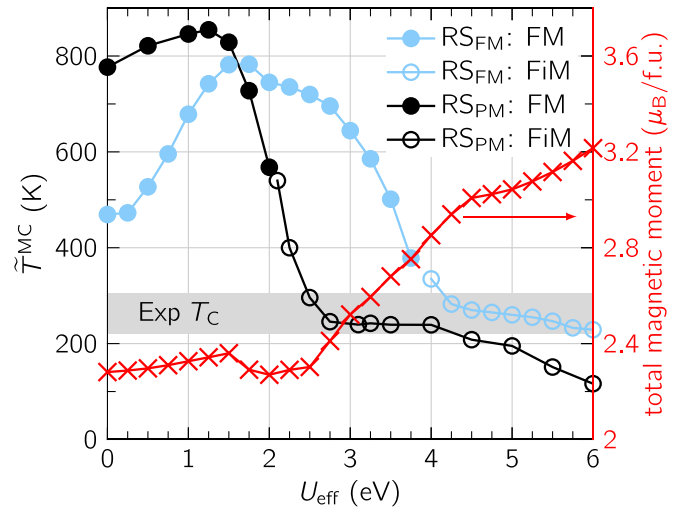


FIG. 8. (Color online) The critical temperatures for the magnetic transition (left axis) and the total magnetic moment per functional unit at the ground state (right axis) as a function of U_{eff} . The MC calculations show a change in the magnetic ground state from clear FM behavior to a FiM situation at $U_{\text{eff}} \approx 2.1$ and 4 eV for the RS_{PM} and RS_{FM} calculations, respectively (see text). The gray shaded area indicates the experimental T_c range.

U_{eff} was already discussed above for the J_{ij} , the larger overlap of the orbitals in the more realistic DLM model. Additionally, the RS_{PM} calculation showed after the kink an almost constant $\tilde{T}^{\text{MC}}(U_{\text{eff}}) = 240$ K for a larger range of U_{eff} parameters (2.75 to 4 eV). On the other side, the ground-state calculation at RS_{FM} with the GF method (GGA + U) returns for $U_{\text{eff}} \approx 5$ eV a \tilde{T}^{MC} inside the experimental range. This observation matches well with the above discussion about the electronic structure and the correspondence of GF method (GGA + U) and VASP (HSE03) calculations at $U_{\text{eff}} \approx 5$ eV (see Fig. 4).

Furthermore, we account in Fig. 8 for the magnetic ground state observed in the MC study with different symbols, having either a FM or FiM ground state. The DLM theory predicted only a FiM ordered ground state for the range of \tilde{T}^{MC} ($U_{\text{eff}} \approx 2.5$ eV) equivalent to experimental results. This is, however, still physically reasonable. While at the critical temperature the induced moments at oxygen might be zero, they will appear at lower temperatures. This leads to a FM ground state obtained with the J_{ij} (RS_{FM}) for even larger U_{eff} (see blue curve in Fig. 8).

On the other hand, the total magnetic moment increases monotonously in the whole U_{eff} range with different linear slopes (see red line in Fig. 8). Only for changing degeneracy for $U_{\text{eff}} > 1.5$ eV the total moment decreases slightly due to a reduction of the induced moments to $0.11\mu_B$ for the two oxygen ions (O_x and O_y), which lie in the same x - y plane as the Co ions. In the following, the linear slope changed around $U_{\text{eff}} \approx 2.5$ eV and $U_{\text{eff}} \approx 4.5$ eV, which correspond to disappearing peaks in the LDOS (see Fig. 6). At the latter U_{eff} , the total moment is $3\mu_B$ and matches well, on the one hand, with the IS-state model and, on the other hand, with the HSE03 calculation in VASP.

We found in summary that the PM model (DLM theory) yields for the critical temperature a good qualitative agreement

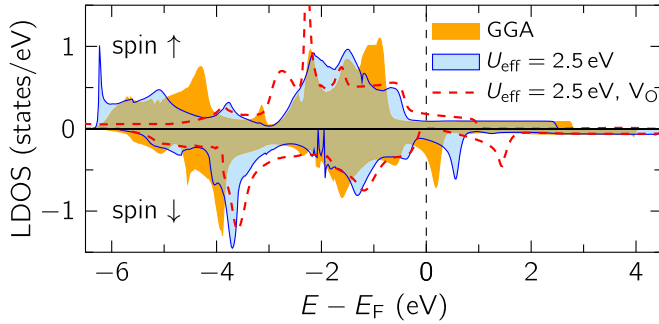


FIG. 9. (Color online) LDOS of the oxygen along the z direction (O_z) for GGA, $U_{\text{eff}} = 2.5$ eV, and with 5 at.% oxygen vacancies (V_O).

with the measurements [1,15] only for a small correlation parameter of $U_{\text{eff}} = 2.50$ to 2.75 eV. Still, an exact comparison with the measured T_C remained complicated due to the different experimental setups, single-crystalline or polycrystalline samples, varying growing techniques, or different oxygen content.

C. Effects of oxygen vacancies

We used the CPA of the GF method to substitute the oxygen sites with a certain concentration of empty spheres, modeling the oxygen vacancies. For a low oxygen deficiency in SCO up to 5 at.%, there is no experimental evidence for an ordering of V_O . Therefore, we assumed randomly distributed oxygen vacancies, which matches well with the concept of the CPA.

The electronic structure of the oxygen ions is mainly dominated by the strong hybridization with the Co d states (see Fig. 3). By including a few atomic percent of oxygen vacancies (5 at.%) in SCO, the unoccupied peak above E_F is shifted to higher energies (see Fig. 9), a similar effect as increasing U_{eff} (see GGA results for comparison in Fig. 9). Both lead to an enhancing orbital localization, either removing effectively oxygen from the lattice or reducing the electron hopping between the Co ions. Anyway, these unoccupied oxygen states can be interpreted as the ligand hole of e_g symmetry, which is expected for the IS state $t_{2g}^4 e_g^1$ [8]. It is stabilized by the ligand hole state $d^6 \underline{L}_{e_g}$ where the hole couples antiferromagnetically to another e_g^{\uparrow} in d^6 : $t_{2g}^4 e_g^2$. We found this configuration also in our LDOS calculation with almost fully occupied orbitals for d^{\uparrow} and t_{2g}^{\downarrow} (see Fig. 6). Although our method is not directly comparable with the dynamic mean-field theory (DMFT) method of Kuneš *et al.* [9], we note that the same spin configuration appeared also in their calculation with the highest multiplet weight.

We calculated again the magnetic transition temperature $\tilde{T}^{\text{MC}}(\delta)$ based on the *ab initio* magnetic exchange coupling constants in RS_{PM} with the MC method but included different amounts of oxygen vacancies δ . Although we observed at the relevant critical temperatures no FM ordering, calculations with the J_{ij} in RS_{FM} revealed a FM ground state at low temperatures for all considered vacancy amounts (not shown). The results were compared with the experimental measurements [1,15]. The experiments with polycrystalline samples [15] varied the oxygen content by ± 6 at.% with respect to the stoichiometric sample and found decreasing T_C with reduced

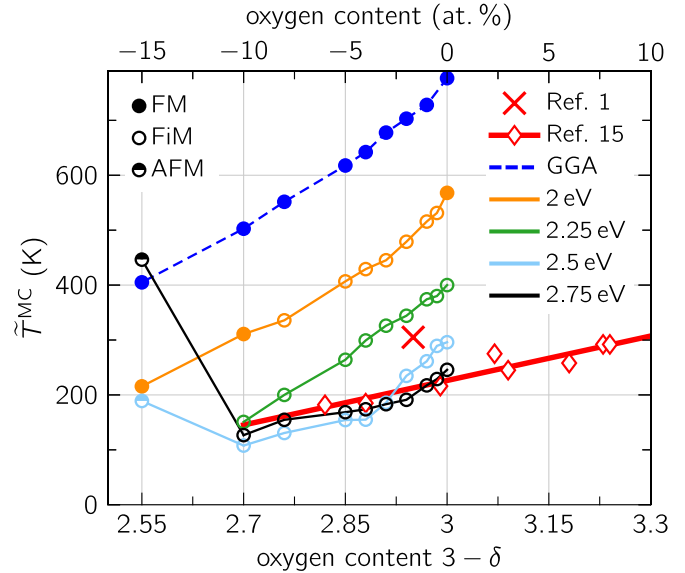


FIG. 10. (Color online) The theoretical critical temperature (DLM model) in dependence of the oxygen content in SCO compared with experimental references. The GGA calculations shown as dashed blue line and GGA + U calculations shown as differently colored solid lines. The open and solid circles in the corresponding colors indicate the calculated data points and the magnetic ground state as shown in Fig. 8. An additional AFM state is marked with a half-filled circle (see text).

oxygen amount (see Fig. 10). A positive value means excess oxygen, which might occupy unknown interstitial sites or form more complicated point defects. This is beyond our aims and we restricted the current study to model only oxygen deficiency by the introduction of oxygen vacancies into the cubic unit cell. In contrast, the single-crystalline T_C was found to be remarkably higher, but the lack of more data points complicates the comparison [1].

In theory, we expected also a reduction of $\tilde{T}^{\text{MC}}(\delta)$, since we found that the localization of the orbitals through oxygen vacancies was like applying an U_{eff} parameter. Therefore, the magnetic interactions in the Co-O-Co bonds were weakened as well. This expectation was generally fulfilled for the calculated $\tilde{T}^{\text{MC}}(\delta)$ at different U_{eff} : the GGA exchange functional alone, $U_{\text{eff}} = 2, 2.25, 2.5$, or 2.75 eV (see Fig. 10). They all show an increase of the critical temperatures by increasing the oxygen content from $\delta = 0.3$ (10 at.%) towards stoichiometric SCO while their slopes varies qualitatively between $U_{\text{eff}} = 2.25$ and 2.5 eV. The slope remained equal for $U_{\text{eff}} = 2.25$ eV and even partially for $U_{\text{eff}} = 2.5$ eV but became for larger U_{eff} reduced and matched well the trend of the experimental results. We note that for $U_{\text{eff}} = 2.5$ eV only the combined effect of U_{eff} and a larger amount of V_O is enough to obtain the experimental trend, whereas $U_{\text{eff}} = 2.75$ eV lies in the region of constant $\tilde{T}^{\text{MC}}(U_{\text{eff}})$. For the latter, the influence of the oxygen vacancies alone to $\tilde{T}^{\text{MC}}(\delta)$ was visible and it agreed well with the measurements (see Fig. 8).

However, these results were just valid in a small range of oxygen-deficiency; otherwise, SCO becomes unstable and forms different structure. This is also visible in the observed magnetic ground states depicted in Fig. 8. At 15 at.% oxygen

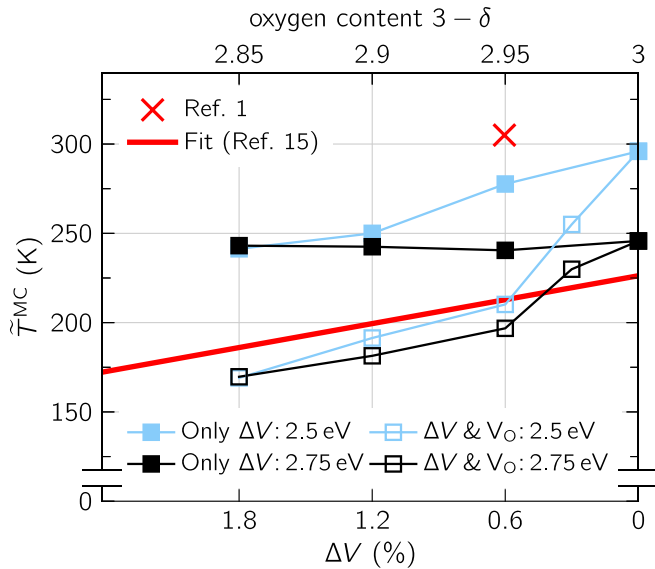


FIG. 11. (Color online) The theoretical critical temperature (DLM model, GGA + U) of SCO in dependence of the volume change ΔV (solid squares, lower axis; reversed to match other figures). The volume change is correlated with the oxygen-deficiency (upper axis) via the experimental results of Ref. [15] (see text). Both effects are also combined (open squares). U_{eff} is 2.5 eV (blue) or 2.75 eV (black), respectively. The magnetic ground state is always FiM.

deficiency and $U_{\text{eff}} \geq 2.5$ eV, the resulting magnetic ground state was AFM. This chemical composition is already close to the ordered brownmillerite structure $\text{SrCoO}_{2.5}$, which is AFM with a high Néel temperature of $T_N = 570$ K [11]. Although the cubic structure is not the appropriate equilibrium structure at this oxygen concentration, the difference in chemical composition might lead already to an AFM order with a higher critical temperature. Such a transition from a FM to an AFM ground state can be caused in SCO, e.g., by strain [10]. A strain, in general, varies the unit cell volume and might therefore modify the magnetic coupling as well.

D. Hydrostatic volume changes

Up to now all calculations were performed with the fixed lattice constant a_{ref} , but measured lattice constants indicate a volume expansion in consequence of oxygen deficiency (see examples in Fig. 2). To estimate the influence of this volume enhancement to the critical temperature $\tilde{T}^{\text{MC}}(\Delta V)$, we choose from Fig. 2 the largest volume expansion as reference [15]. Therefore, we scaled the lattice parameters of the cubic unit cell for defect-free SCO up to 1.8% and calculated \tilde{T}^{MC} in RSPM (see solid squares and the lower axis in Fig. 11). For

$U_{\text{eff}} = 2.5$ eV, the increasing distance between the Co atoms reduces their magnetic interaction and the critical temperature, again similar to U_{eff} or V_{O} . Hence, $\tilde{T}^{\text{MC}}(\Delta V)$ remains for $U_{\text{eff}} = 2.75$ eV almost constant.

On the other hand, the volume expansion is correlated to a particular oxygen content (see Fig. 2). For simplicity, it is linearly interpolated from Ref. [15] to derive in Fig. 11 the upper axis (open squares). The combination of volume expansion and oxygen deficiency leads for $U_{\text{eff}} = 2.5$ eV to a similar quantitative curve as for $\tilde{T}^{\text{MC}}(\delta)$ but the observed kink appears already for $\delta = 0.05$ or $\Delta V = 0.6\%$, respectively. In contrast, the qualitative and quantitative agreement of the variation of \tilde{T}^{MC} for $U_{\text{eff}} = 2.75$ eV is still in place. Finally, we note that although the good agreement with Ref. [15] of the theoretically obtained \tilde{T}^{MC} , the variation ΔV was the upper boundary of Fig. 2. For example, in Ref. [18] the oxygen-deficiency of $\delta = 0.16$ with respect to their value at $\delta = 0$ is correlated to a much smaller volume expansion of $\Delta V = 0.6\%$. As a result the slope of $\tilde{T}^{\text{MC}}(\delta)$ changes drastically as well.

IV. CONCLUSIONS

We conclude that for cubic SCO the inclusion of temperature effects via the DLM model and a small correlation correction parameter of $U_{\text{eff}} \approx 2.75$ eV is necessary to describe the measured magnetic properties, such as the magnetic moment or, in particular, the Curie temperature. Such values of U_{eff} are expected for a metallic system. In the studied compound, we observe mainly the band magnetism, which is reduced by oxygen-mediated superexchange. Furthermore, our calculations agree with the atomic multiplet calculations and the picture of the IS state of Potze *et al.* [8].

On the other hand, oxygen vacancies can drastically alter the magnetic properties [15]. The simple means of the CPA were successful to model qualitatively and quantitatively the experimentally observed reduction of \tilde{T} induced by oxygen vacancies [15]. They are one of the most important types of defects in oxides; even single crystalline samples might be not completely stoichiometric [1]. The randomly distributed vacancies weaken the Co-O-Co bonds and reduce the exchange coupling, similar to electronic correlations. The same behavior was also observed for a possible increase of the unit cell volume.

ACKNOWLEDGMENTS

This work was funded by the Deutsche Forschungsgemeinschaft DFG within SFB 762, “Functionality of Oxide Interfaces.” We gratefully acknowledge fruitful discussions with Igor V. Maznichenko and Alberto Marmodoro.

- [1] Y. Long, Y. Kaneko, S. Ishiwata, Y. Taguchi, and Y. Tokura, Synthesis of cubic SrCoO_3 single crystal and its anisotropic magnetic and transport properties, *J. Phys.: Condens. Matter* **23**, 245601 (2011).
 [2] P. Shuk, A. Vecher, V. Kharton, L. Tichonova, H. Wiemhöfer, U. Guth, and W. Göpel, Electrodes for oxygen sensors based on

rate earth manganites or cabaltites, *Sens. Actuators B* **16**, 401 (1993).

- [3] T. Inagaki, K. Miura, H. Yoshida, R. Maric, S. Ohara, X. Zhang, K. Mukai, and T. Fukui, High-performance electrodes for reduced temperature solid oxide fuel cells with doped lanthanum gallate electrolyte, *J. Power Sources* **86**, 347 (2000).

- [4] B. Lin, S. Wang, H. Liu, K. Xie, H. Ding, M. Liu, and G. Meng, SrCo_{0.9}Sb_{0.1}O_{3- δ} cubic perovskite as a novel cathode for intermediate-to-low temperature solid oxide fuel cells, *J. Alloys Comp.* **472**, 556 (2009).
- [5] S. Mathi Jaya, R. Jagadish, R. S. Rao, and R. Asokamani, Electronic structure and magnetism of SrFeO₃ and SrCoO₃, *Phys. Rev. B* **43**, 13274 (1991).
- [6] M. Zhuang, W. Zhang, A. Hu, and N. Ming, Possible magnetic ground state in the perovskite SrCoO₃, *Phys. Rev. B* **57**, 13655 (1998).
- [7] H.-P. Wu, D.-G. Chen, D.-C. Huang, and K.-M. Deng, Electronic and magnetic properties of SrCoO₃: The first principles study, *Acta Phys. Sin.* **61**, 037101 (2012).
- [8] R. H. Potze, G. A. Sawatzky, and M. Abbate, Possibility for an intermediate-spin ground state in the charge-transfer material SrCoO₃, *Phys. Rev. B* **51**, 11501 (1995).
- [9] J. Kuneš, V. Křápek, N. Parragh, G. Sangiovanni, A. Toschi, and A. V. Kozhevnikov, Spin State of Negative Charge-Transfer Material SrCoO₃, *Phys. Rev. Lett.* **109**, 117206 (2012).
- [10] J. H. Lee and K. M. Rabe, Coupled Magnetic-Ferroelectric Metal-Insulator Transition in Epitaxially Strained SrCoO₃ from First Principles, *Phys. Rev. Lett.* **107**, 067601 (2011).
- [11] T. Takeda and H. Watanabe, Magnetic Properties of the System SrCo_{1-x}Fe_xO_{3-y}, *J. Phys. Soc. Jpn.* **33**, 973 (1972).
- [12] H. Taguchi, M. Shimada, and M. Koizumi, Magnetic properties in the system La_{1-x}Sr_xCoO₃ (0.5 \leq x \leq 1.0), *Mater. Res. Bull.* **13**, 1225 (1978).
- [13] P. Bezdicka, A. Wattiaux, J. C. Grenier, M. Pouchard, and P. Hagemuller, Preparation and characterization of fully stoichiometric SrCoO₃ by electrochemical oxidation, *Z. Anorg. Allg. Chem.* **619**, 7 (1993).
- [14] S. Kawasaki, M. Takano, and Y. Takeda, Ferromagnetic properties of SrFe_{1-x}Co_xO₃ synthesized under high pressure, *J. Solid State Chem.* **121**, 174 (1996).
- [15] S. Balamurugan, K. Yamaura, A. B. Karki, D. P. Young, M. Arai, and E. Takayama-Muromachi, Specific-heat evidence of strong electron correlations and thermoelectric properties of the ferromagnetic perovskite SrCoO_{3- δ} , *Phys. Rev. B* **74**, 172406 (2006).
- [16] L. Karvonen, S. Räsänen, H. Yamauchi, and M. Karppinen, Chemical oxidation of SrCoO_{3- δ} , *Chem. Lett.* **36**, 1176 (2007).
- [17] S. Balamurugan, Impact of high pressure and high temperature on annealed oxygen-deficient CoSrO_{3- δ} perovskites: Structural and magnetization studies, *J. Supercond. Novel. Magn.* **23**, 225 (2009).
- [18] R. Le Toquin, W. Paulus, A. Cousson, C. Prestipino, and C. Lamberti, Time-resolved in situ studies of oxygen intercalation into SrCoO_{2.5}, performed by neutron diffraction and X-ray absorption spectroscopy, *J. Am. Chem. Soc.* **128**, 13161 (2006).
- [19] L. Karvonen, H. Yamauchi, and M. Karppinen, Homologous series of SrCoO_{(3n-1)/n} perovskites obtained through Br₂ oxygenation of SrCoO_{2.5}, *Chem. Mater.* **20**, 7143 (2008).
- [20] A. Nemudry, P. Rudolf, and R. Schöllhorn, Topotactic electrochemical redox reactions of the defect perovskite SrCoO_{2.5+x}, *Chem. Mater.* **4756**, 2232 (1996).
- [21] H. Taguchi, M. Shimada, and M. Koizumi, The effect of oxygen vacancy on the magnetic properties in the system SrCoO_{3- δ} (0 < δ < 0.5), *J. Solid State Chem.* **29**, 221 (1979).
- [22] K. Momma and F. Izumi, VESTA 3 for three-dimensional visualization of crystal, volumetric and morphology data, *J. Appl. Crystall.* **44**, 1272 (2011).
- [23] G. Kresse and J. Hafner, *Ab initio* molecular-dynamics simulation of the liquid-metal-amorphous-semiconductor transition in germanium, *Phys. Rev. B* **49**, 14251 (1994).
- [24] G. Kresse and J. Furthmüller, Efficiency of *ab-initio* total energy calculations for metals and semiconductors using a plane-wave basis set, *Comp. Mater. Sci.* **6**, 15 (1996).
- [25] J. Hafner, *Ab-initio* simulations of materials using VASP: Density-functional theory and beyond, *J. Comp. Chem.* **29**, 2044 (2008).
- [26] M. Lüders, A. Ernst, W. M. Temmerman, Z. Szotek, and P. J. Durham, *Ab initio* angle-resolved photoemission in multiple-scattering formulation, *J. Phys.: Condens. Matter* **13**, 8587 (2001).
- [27] J. P. Perdew, K. Burke, and M. Ernzerhof, Generalized Gradient Approximation Made Simple, *Phys. Rev. Lett.* **77**, 3865 (1996).
- [28] V. I. Anisimov, J. Zaanen, and O. K. Andersen, Band theory and Mott insulators: Hubbard U instead of Stoner I , *Phys. Rev. B* **44**, 943 (1991).
- [29] S. L. Dudarev, G. A. Botton, S. Y. Savrasov, C. J. Humphreys, and A. P. Sutton, Electron-energy-loss spectra and the structural stability of nickel oxide: An LSDA+ U study, *Phys. Rev. B* **57**, 1505 (1998).
- [30] J. Heyd, G. E. Scuseria, and M. Ernzerhof, Hybrid functionals based on a screened Coulomb potential, *J. Chem. Phys.* **118**, 8207 (2003).
- [31] A. I. Liechtenstein, M. I. Katsnelson, V. P. Antropov, and V. A. Gubanov, Local spin density functional approach to the theory of exchange interactions in ferromagnetic metals and alloys, *J. Magn. Magn. Mater.* **67**, 65 (1987).
- [32] S. Tyablikov, *Methods in the Quantum Theory of Magnetism* (Springer, Berlin, Heidelberg, 1995).
- [33] G. Fischer, M. Däne, A. Ernst, P. Bruno, M. Lüders, Z. Szotek, W. Temmerman, and W. Hergert, Exchange coupling in transition metal monoxides: Electronic structure calculations, *Phys. Rev. B* **80**, 014408 (2009).
- [34] M. M. Otrokov, A. Ernst, S. Ostanin, G. Fischer, P. Buczek, L. M. Sandratskii, W. Hergert, I. Mertig, V. M. Kuznetsov, and E. V. Chulkov, Intralayer magnetic ordering in Ge/Mn digital alloys, *Phys. Rev. B* **83**, 155203 (2011).
- [35] M. M. Otrokov, A. Ernst, V. V. Tugushev, S. Ostanin, P. Buczek, L. M. Sandratskii, G. Fischer, W. Hergert, I. Mertig, V. M. Kuznetsov, and E. V. Chulkov, *Ab initio* study of the magnetic ordering in Si/Mn digital alloys, *Phys. Rev. B* **84**, 144431 (2011).
- [36] J. Staunton, B. Gyorffy, A. Pindor, G. Stocks, and H. Winter, The “disordered local moment” picture of itinerant magnetism at finite temperatures, *J. Magn. Magn. Mater.* **45**, 15 (1984).
- [37] B. L. Gyorffy, A. J. Pindor, J. B. Staunton, G. M. Stocks, and H. Winter, A first-principles theory of ferromagnetic phase transitions in metals, *J. Phys. F: Met. Phys.* **15**, 1337 (1985).
- [38] P. Soven, Coherent-potential model of substitutional disordered alloys, *Phys. Rev.* **156**, 809 (1967).
- [39] B. Györffy, Coherent-potential approximation for a nonoverlapping-Muffin-Tin-potential model of random substitutional alloys, *Phys. Rev. B* **5**, 2382 (1972).